Substrate Dependence of the Self-Heating in Lead Zirconate Titanate (PZT) MEMS Actuators

Yiwen Song[1], Kyuhwe Kang[1], Pannawit Tipsawat[2], Christopher Y. Cheng[2], Wanlin Zhu[2], Michael LaBella[2], Sukwon Choi[1,a)], and Susan E. Trolier-McKinstry[2,a)]
[1]Department of Mechanical Engineering, The Pennsylvania State University
University Park, PA, 16802
[2]Department of Materials Science and Engineering and Materials Research Institute, The Pennsylvania State University
University Park, PA, 16802

Abstract: Lead zirconate titanate (PZT) thin films offer advantages in microelectromechanical systems (MEMS) including large motion, lower drive voltage, and high energy densities. Depending on the application, different substrates are sometimes required. Self-heating occurs in PZT-MEMS due to the energy loss from domain wall motion which can degrade the device performance and reliability. In this work, the self-heating of PZT thin films on Si and glass and a film released from a substrate were investigated to understand the effect of substrates on the device temperature rise. Nano-particle assisted Raman thermometry was employed to quantify the operational temperature rise of these PZT actuators. The results were validated using a finite element thermal model, where the volumetric heat generation was experimentally determined from the hysteresis loss. While the volumetric heat generation of the PZT films on different substrates were similar, the PZT films on Si substrate shows minimal temperature rise due to the effective heat dissipation through the high thermal conductivity substrate. The temperature rise on the released structure is 6.8× higher than that on the glass substrates due to the absence of vertical heat dissipation. Experimental and modeling results show that the thin layer of residual Si remaining after etching plays a crucial role in mitigating the effect of device self-heating. The outcomes of this study suggest that high thermal conductivity passive-elastic layers can be used as an effective thermal management solution for PZT-based MEMS actuators.

Keywords: Device self-heating, Lead zirconate titanate (PZT), piezoelectric MEMS actuators, Raman thermometry, substrate effects

[a)] Authors to whom correspondence should be addressed: sukwon.choi@psu.edu (Sukwon Choi), stmckinstry@psu.edu (Susan Trolier-McKinstry)

Introduction

Lead zirconate titanate (PZT) is a ferroelectric material that exhibits a higher piezoelectric coefficient (d_{33}) and larger electromechanical coupling factor than those for $BaTiO_3$ and $K_{1-x}Na_xNbO_3$. PZT-based devices are utilized in a wide range of technologies, enabling precise and responsive actuation, sensing, and energy harvesting applications.[1–4] However, self-heating in PZT can degrade the device reliability, especially in applications with large electric-field excitation or high-power operation. For example, excessive operational temperature rise can lead to reduced efficiency, drift in piezoelectric properties[5], material degradation due to thermal stress[6], and shift in the resonance frequencies of sensors and resonators[7,8]. Typically, actuators are intentionally limited to self-heating up to 20˚C above ambient temperature, in order to avoid changes in the domain structure.[9] Heat generation mechanisms in bulk PZT ceramics have been

discussed in the literature.[9–11] Notably, heat generation was found to be caused by hysteresis loss due to domain wall motion. Domain walls act as boundaries that separate regions with different polarization orientations; their motion under applied electric fields leads to localized frictional heating. While self-heating in bulk PZT materials is well-understood, studies on the self-heating in PZT thin film-based MEMS structures are lacking.

PZT thin films in microelectromechanical systems (MEMS) can generate large motions; when the domain states are properly stabilized, they can also show low hysteresis, and high energy densities.[12] PZT thin films can be deposited on a variety of substrates such as Si[13], glass[14,15], metals[16,17], and $SrTiO_3$[18], which allows a range of mechanical and electrical performance in the elastic layer for piezoelectric MEMS devices.

The self-heating behavior in PZT thin films differs from that in PZT bulk ceramics in several aspects. First, PZT thin films often have restricted domain wall motion due to small grain size, high residual stress imposed by the substrate, and/or a high concentration of point and line defects.[19] Second, heat extraction from the film depends on the thermal conductivity of the substrate material and the structure of the device. Lundh et al. reported considerable self-heating in released PZT MEMS actuators under various driving conditions including multiple combinations of frequencies, AC amplitudes, and DC offsets.[20] Fragkiadakis et al. combined simulations and measurements of self-heating in PZT MEMS actuator arrays; they observed a temperature rise exceeding 100°C when closely spaced actuators operated simultaneously.[21] Both studies show the impact of driving conditions on self-heating in commercial PZT MEMS with released structures. This work aims to understand how substrate and device structure influences self-heating behavior in PZT film-based MEMS. Therefore, in this study, clamped PZT films were fabricated on Si and glass substrates and thermal excursions as a function of electrical excitation were examined using nanoparticle-assisted Raman thermometry. Additionally, a released structure was prepared. Results were validated and interpreted using device thermal modeling.

Device Fabrication

To investigate the heat dissipation on various substrates, PZT test structures were fabricated on Si and glass substrates, as shown in Fig. 1(a). In addition, released structures were prepared.

For PZT film on glass, a stack of 30 nm Ti and 100 nm Pt was deposited on 400 μm thick Corning Eagle glass. A commercial 114/52/48/2 solution of $PbZr_{0.52}Ti_{0.48}O_3$ from Mitsubishi Materials Corporation was used for PZT film deposition. The solution was spun on at 2750 RPM for 30 seconds. The film was pyrolyzed at 100°C for 2 minutes and then at 300°C for 8 minutes. The film underwent crystallization processes, first at 520°C for 1 minute followed by ramping to 650°C at a rate of 3°C/second (a slow ramp rate was used to prevent the glass wafer from deforming or shattering); subsequently, the film was held at 650°C for 2 minutes. The crystallization processes were performed with a 2 sccm O_2 flow in a lead-rich rapid thermal annealer.[22] The process was repeated until a total PZT thickness of 0.98 μm was achieved. Subsequently, the top electrodes (3 nm of Ti and 100 nm of Pt) were deposited at room temperature via DC magnetron sputter deposition without breaking the vacuum. These were then

patterned into circular shaped electrodes using the lift-off process. A schematic of the completed structure on glass substrate is shown in Figure 1 (b).

The detailed deposition process for PZT on Si used in this study has been described elsewhere.[23] The PZT film on Si and the released structure were fabricated on the same 4-inch Si wafer. The PZT film was deposited on a commercial platinized Si wafer with 1 μm of SiO_2 thermal oxide. 20 nm Ti and 150 nm Pt were deposited as the bottom electrode. The solution and spinning conditions used were similar to those previously described. The film was pyrolyzed at 100 °C for 1 minute and at 300 °C for 4 minutes, followed by crystallization at 700°C thermal annealing with 2 sccm O_2 flow for 1 minute. The process was repeated until a total PZT thickness of 1.08 μm was achieved. Then, the top electrode was deposited and patterned through a lift-off process similar to that of the glass substrate sample.

Following this, an Al_2O_3 insulator pad was deposited using thermal atomic layer deposition on a commercial Kurt-Lesker ALD 150LE (Kurt J. Lesker, Pennsylvania, USA) system at 150°C, employing tetramethylammonium hydroxide (TMAH) and H_2O as precursors. The Al_2O_3 thin film underwent lithographic patterning and was wet-etched (using a TMAH-based developer and CD-26) into a rectangular insulating pad. The contact pad, consisting of 3 nm of Ti and 100 nm of Pt, was deposited and patterned using a process similar to that of the top electrode. The metal pad was positioned on top of an Al_2O_3 pad to insulate it from the PZT thin film. Finally, the Pt bottom electrode was exposed by wet etching the PZT thin film into a rectangular shape using a mixed solution of hydrochloric acid, 6:1 buffered oxide etchant, and deionized water. A schematic of the completed structure on Si is shown in Figure 1 (c).

To prepare a released PZT film, SiO_2 was removed on the back side by submerging the sample in a 6:1 buffered oxide etch (BOE) solution at room temperature, while the front side was protected with a blanket photoresist. After etching, the sample was cleaned in acetone, isopropyl alcohol, and deionized water. Then, the front side was coated with ProTEK B3 as a protective layer. Deep reactive ion etching (DRIE) was performed in a DSi-V Deep Silicon Etch system (SPTS, Newport, USA) using the Bosch process at 3°C; thick AZ4620 photoresist was utilized as a soft mask. For the release process, the sample was etched until the trench reached the buried SiO_2 layer. It is important to note that the diaphragm is delicate due to the low thickness and the choice not to use a passive elastic support. Fully removing the Si without breaking the diaphragm proved challenging. Thus, residual Si on the trench edges at the backside of the diaphragm can be seen in some devices, as depicted in Figure 1 (d). Figure 1 (e) shows scanning electron microscopy (SEM) images of the cross-section of the released structure. The residual Si thickness on this structure measured 170 nm. It is noted that the remaining Si thickness varied along the radius of the wafer.

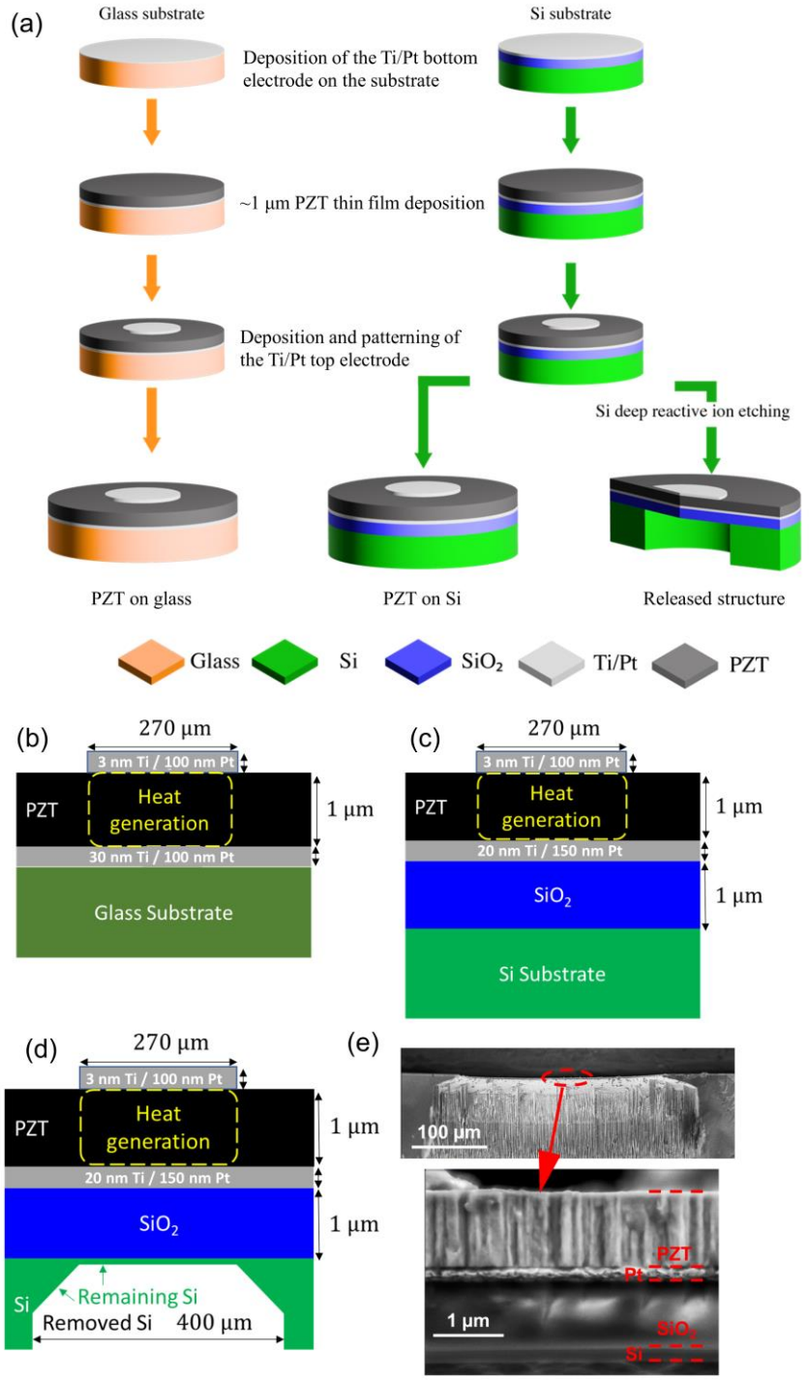

Figure 1. (a) The device fabrication process that illustrates preparation of the bottom electrode on a substrate, deposition of a blanket PZT thin film, and lift-off/patterning of the top electrode. The deposition and patterning of the Al_2O_3 insulator and Ti/Pt contact pads are not shown in this figure. Schematics of PZT on (b) glass, (c) Si, and (d) a released structure (not to scale). (e) Cross-sectional SEM images of the PZT film released from a Si substrate.

Thermal Characterization

Raman thermometry allows *in situ* characterization of device self-heating with a sub-micrometer resolution by monitoring changes in the optical phonon energy (or frequency) using a monochromatic laser excitation source.[24–26] In practice, the lattice temperature rise is estimated based on the spectral features of the Raman peaks including peak position, line width, and anti-Stokes/Stokes Raman intensity ratio. Standard Raman thermometry has been demonstrated for the thermal characterization of microelectronics based on materials with well-defined Raman peaks such as Si[27] and GaN[25,28]. However, the characteristic Raman peaks of PZT are too broad to track the small changes in peak position and linewidth essential to estimate the temperature rise, as shown in Figure 2 (a). In addition, the crystal's phonon energy is a function of temperature and film stress, which change periodically under AC driving conditions; moreover, the top electrode blocked visual access to the film. Therefore, nanoparticle-assisted Raman thermometry [29,30] was used. Anatase titanium dioxide (TiO_2) nanoparticles (with 99.98% purity and ~200 nm individual size) were deposited on the surface of the top electrodes, serving as a temperature probe. As shown in Figure 2 (b), TiO_2 nanoparticles exhibit a well-defined Raman peak (i.e., the E_g phonon mode with a frequency of ~143 cm^{-1} at room temperature) that are highly sensitive to changes in temperature[30]. This allowed precise temperature measurements. Notably, temperature values deduced from the use of TiO_2 nanoparticles are free from thermoelastic stress effects because the thermal expansion of the nanoparticles is not restricted by the underlying surface.[31]

Details of the Raman setup and experimental procedures have been previously reported by Lundh[31]; a concise summary is provided here for reference. A LabRAM HR Evolution spectrometer (Horiba, New Jersey, USA) equipped with a 532 nm laser source and 1800 grooves/mm grating, and a 50× long working distance objective (NA=0.45) was used for Raman thermometry experiments. To prevent laser-induced heating of both the TiO_2 nanoparticles and the underlying top electrode, a laser power of ~1 mW was used. A reference mercury emission line at approximately 546 nm was continuously monitored to account for instrument drift (i.e., systematic errors/offsets in the measured Raman spectra) attributed to room temperature fluctuations. To apply an AC electric field to the device, a DS345 (Stanford Research Systems, California, USA) function generator was used to control the operational frequency and DC offset of an AT Techron 7228 amplifier (AE Techron, Indiana, USA) that managed the output voltage amplitude.

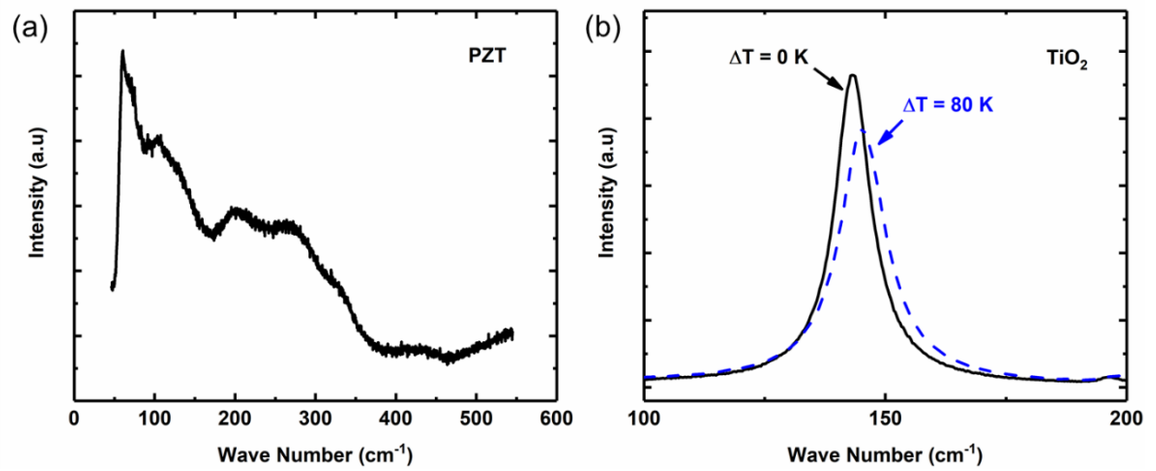

Figure 2: (a) Raman spectra of PZT, (b) The Raman peaks of the E_g phonon mode of TiO_2 nanoparticles at different temperatures.

Electrical Characterization and Device Modeling

3D finite element analysis (FEA) thermal modeling of the PZT MEMS devices was performed using COMSOL Multiphysics to account for heat dissipation through the device structure. Room temperature thermal conductivity values were used in the simulation due to the relatively small amount of self-heating (< 20 K).

Heat generation in PZT is known to be mainly caused by hysteresis loss due to domain wall motion.[9,10] Therefore, the volumetric heat generation per cycle was experimentally determined from the area enclosed by the polarization-electric field (P-E) loops. The power density (Q) was determined by multiplying the frequency by the heat generation per cycle.[21]

$$Q = f \times \int E \, dP$$

where f is the frequency, E is the electric field, and P is the polarization. The films underwent a large number of cycles (~3 million cycles) due to the high frequency and long acquisition time required to perform the NP Raman measurement. Thus, the magnitude of hysteresis loss may change during the cycles due to fatigue.[32] Therefore, P-E loops of both fresh films and films after cycling were measured. Self-heating was calculated using both values to account for the possible temperature range at different points in the fatigue cycle. Representative P-E loops for fresh and fatigued films driven by a 10 kHz sinusoidal waveform with an amplitude of 250 kV/cm for PZT on glass, Si, and the released structure are shown in Figure 3 (a), (b), and (c), respectively. It should be noted that the films were prone to failure under large fields and high frequencies; therefore, the maximum field used for thermal study was limited to a relatively low magnitude of 150 kV/cm. A summary of the test conditions and their corresponding heat generation rates is shown in Table 1.

Since the devices had a circular top electrode, rotational axial symmetry was applied to the model to mitigate computational costs. An isothermal boundary condition was imposed at the bottom of the substrate (to mimic the experimental setup where the devices were placed on a temperature-controlled stage), and natural convection was applied to all other surfaces. A mesh

convergence study was performed to confirm that the results did not change at higher mesh densities.

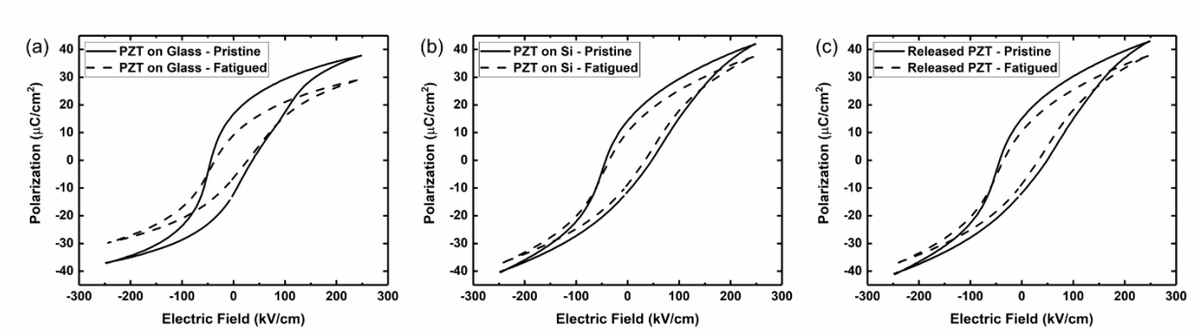

Figure 3: The P-E loop characterization results at a frequency of 10 kHz (sinusoidal waveform) of the PZT films on (a) a glass substrate, (b) a Si substrate, and (c) a released structure. The pristine loops were measured before cycling and the fatigued loops were measured after 1×10^6 cycles.

Table 1: The calculated power densities (GW/m^3) from fatigued P-E loops at 10 kHz

	50 kV/cm	100 kV/cm	150 kV/cm
PZT on glass	1.3	8.3	16.9
PZT on Si	1.4	8.5	19.2
PZT fully released	1.4	8.4	19.6

Results and Discussion

Figure 4 compares the temperature rise of PZT films on glass and Si substrates and two fully released films when operated under a 10 kHz bipolar AC electric field. Measurement data acquired from nanoparticle-assisted Raman thermometry was in good agreement with the FEA thermal modeling results. While no significant temperature rise occurred in the PZT films on a Si substrate, clear evidence of device self-heating was observed for the PZT films on a glass substrate. Notably, the measured power densities of the PZT films on Si and on glass substrates are comparable, especially prior to the fatigue cycles. The discrepancy in device self-heating was caused by the different thermal conductivity of the Si (~130 W/mK at room temperature) and glass (~1 W/mK) substrates. While a similar amount of heat (19.2 GW/m^3 and 16.9 GW/m^3) was generated in both cases, the Si substrate effectively removed heat from the active region and

acted as an effective heat sink, resulting in a negligible device temperature rise.

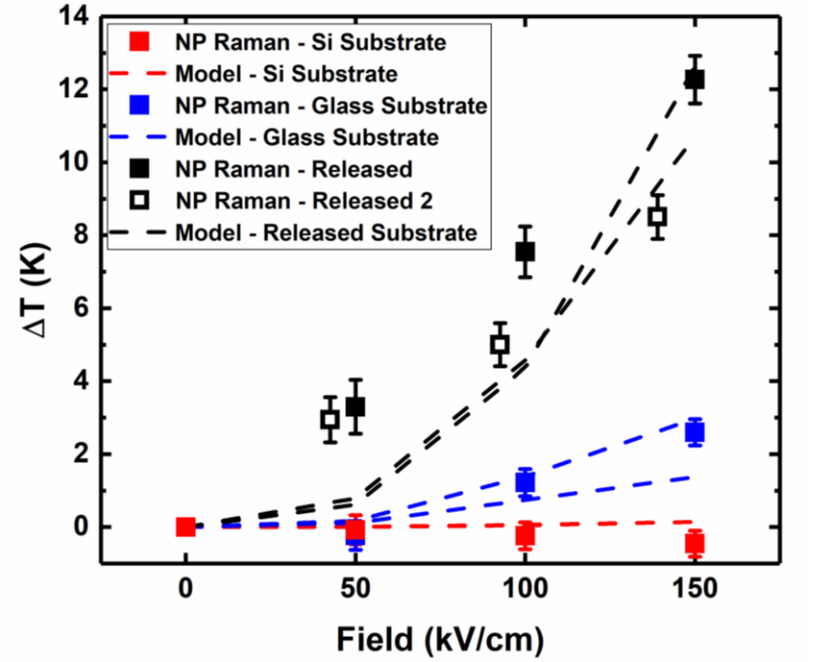

Figure 4. The temperature rise of PZT on Si, PZT on glass, and two fully released PZT devices operated with a 10 kHz bipolar field. The modeling results are bounded by two dashed lines: the upper and lower lines correspond to results based on the P-E loops (i.e., measured heat generation rates) of fresh and fatigued devices, respectively. The self-heating in PZT on Si is negligible. The negative temperature results (~ -0.5 K) are attributed to room temperature fluctuation.

No significant changes were observed in the P-E loop between the released film and the film on Si, indicating negligible change in the global stress state. Upon fully release of the PZT film from the Si substrate, the heat dissipation became markedly less effective, leading to more intense device self-heating. As illustrated in Figure 4, a much larger increase in temperature was observed in the fully released films as compared to the films on solid substrates. Two fully released structures were tested to account for random errors caused by room temperature fluctuations and local variations in the film quality. While the measured temperatures and the modeling results agree well under high field conditions, a notable difference is observed under low field operation. This discrepancy may have resulted from additional heating mechanisms such as Joule heating in the electrode. The effect of such heating mechanisms would become more noticeable under low field operation because of the relatively low hysteresis loss that is manifested by the small P-E loop area. Conversely, under higher field operation (e.g., 150 kV/cm), the hysteresis loss is the dominant heat generation mechanism, resulting in a closer agreement between the measured temperature rise and the modeling results (that are purely based on the hysteresis loss). Simulation results suggest that the peak temperature rise of a fully released device will be 6.8× higher (under 150 kV/cm operation) than that of a film on a glass substrate. Therefore, fully released piezoelectric MEMS structures will be prone to thermal reliability issues and more exacerbated self-heating is expected to occur in actuator arrays as reported by Fragkiadakis *et. al.*[21].

As discussed in the fabrication section, the DRIE process produces non-uniform etching across the wafer. Because there is no hard etch stop, there is some residual Si underneath the released diaphragm; the thickness of the remaining Si layer varied depending on the location. The exact thickness of the remaining Si was measured using cross-sectional SEM on multiple devices across the wafer. Near the center of the wafer where the etch rate was slower, the Si thickness was a few hundred nanometers thicker.

Therefore, it is crucial to understand the impact of the remaining Si thickness on device thermal performance. Additional NP Raman measurement and modeling were performed on a device with 170 nm of Si remaining. A higher field (200 kV/cm) and a higher frequency (20 kHz) were used. A temperature rise of 12.2 ± 1.6 K was detected using Raman thermometry.

A parametric sweep of the remaining Si thickness was performed (using the device thermal model) to evaluate its effect on device self-heating. As depicted in Figure 5, when Si is completely removed, the temperature rise in the PZT film exceeds 25°C under 200 kV/cm bipolar AC electric field operation at a frequency of 20 kHz. This produced an experimental power density of 91.8 GW/m^3. The film's thermal response was highly sensitive to the remaining Si thickness. This was attributed to the lower thermal conductance of the PZT film as compared to Si; that is, the remaining Si layer transferred heat away from the device active region more effectively. Consequently, the device temperature rise was substantially smaller, even with a thin layer of Si remaining. For example, 200 nm thick residual Si reduced the temperature rise by over 50% as compared to a fully released case. This suggests that the Si layer utilized in most SOI-based piezoelectric MEMS is critical for effective thermal management. It is important to note that this study is based on a single device. In the case of actuator arrays, such as in the case of a piezoelectric inkjet print head, the temperature rise is amplified due to thermal crosstalk.[21] For such applications, inclusion of a high thermal conductivity passive elastic layer behind the active piezoelectric film may significantly improve the thermal performance at both device- and system-levels.

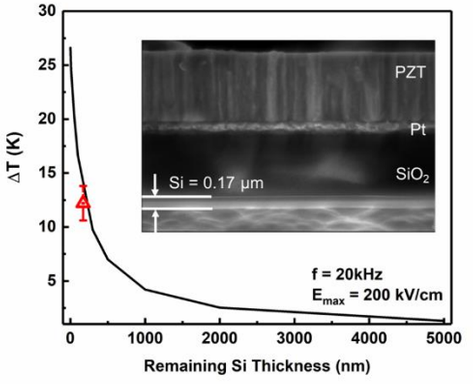

Figure 5. The device temperature rises as a function of the remaining Si thickness. The image insert shows a device structure with 170 nm of Si remaining below the PZT film. This device was tested via Raman thermometry and the red marker shows the measurement results (12.2 ± 1.6 K).

Conclusions

The self-heating behavior of lead zirconate titanate (PZT) thin films fabricated on glass and Si substrates as well as a released structure were measured using nanoparticle-assisted Raman thermometry. The results show that PZT thin films on a Si substrate exhibit a minimal temperature rise, attributed to the high thermal conductivity of the substrate material. In contrast, PZT thin films on a glass substrate exhibit notable self-heating due to the two orders of magnitude lower thermal conductivity of glass limiting vertical heat extraction from the device active region. When the PZT film is fully released from a Si substrate, the device temperature rise exceeds that of a PZT film on glass by 6.8× under the highest electric field test condition (150 kV/cm). Both experimental and simulation results suggest that a residual Si layer underneath the PZT film can significantly reduce the film temperature rise caused by device self-heating. These findings highlight that the choice of the passive elastic layer of PZT MEMS actuator arrays (in terms of the thermal conductivity and thickness of the layer) strongly influences effective thermal management at both device- and system-levels.

Acknowledgements

This material is based upon work supported by the National Science Foundation, as part of the Center for Dielectrics and Piezoelectrics under Grant Nos. IIP-1361571, IIP-1361503, IIP-1841453, and IIP-1841466.

Data Availability

The data that support the findings of this study are available from the corresponding author upon reasonable request.

Reference

[1] S. Priya, "Criterion for material selection in design of bulk piezoelectric energy harvesters," IEEE Trans Ultrason Ferroelectr Freq Control **57**(12), 2610–2612 (2010).
[2] P. Janphuang, R. Lockhart, N. Uffer, D. Briand, and N.F. de Rooij, "Vibrational piezoelectric energy harvesters based on thinned bulk PZT sheets fabricated at the wafer level," Sens Actuators A Phys **210**, 1–9 (2014).
[3] Y. Qiu, J. V Gigliotti, M. Wallace, F. Griggio, C.E.M. Demore, S. Cochran, and S. Trolier-McKinstry, "Piezoelectric Micromachined Ultrasound Transducer (PMUT) Arrays for Integrated Sensing, Actuation and Imaging," Sensors **15**(4), 8020–8041 (2015).
[4] P. Muralt, R.G. Polcawich, and S. Trolier-McKinstry, "Piezoelectric Thin Films for Sensors, Actuators, and Energy Harvesting," MRS Bull **34**(9), 658–664 (2009).
[5] M H Lente, J A Eiras, M.H. Lente, and J.A. Eiras, "Interrelationship between self-heating and ferroelectric properties in PZT ceramics during polarization reorientation," Journal of Physics: Condensed Matter **12**(27), 5939 (2000).
[6] M. Stewart, and M.G. Cain, "Measurement and modelling of self-heating in piezoelectric materials and devices," in Characterisation of Ferroelectric Bulk Materials and Think Films edited by M.G. Cain (Springer Netherlands, Dordrecht, 2014), pp. 147–189.
[7] S. Yan, C. Sun, Q. Cui, M. He, Willhandy, R. Wang, J. Hao, and X. Chu, "Dielectric, piezoelectric and dc bias characteristics of Bi-doped PZT multilayer ceramic actuator," Mater Chem Phys **255**, 123605 (2020).

[8] Z. Wu, and S. Cochran, "Loss effects on adhesively-bonded multilayer ultrasonic transducers by self-heating," Ultrasonics **50**(4), 508–511 (2010).
[9] K. Uchino, J.H. Zheng, Y.H. Chen, X.H. Du, J. Ryu, Y. Gao, S. Ural, S. Priya, and S. Hirose, "Loss mechanisms and high power piezoelectrics," J Mater Sci **41**(1), 217–228 (2006).
[10] J. Zheng, S. Takahashi, S. Yoshikawa, K. Uchino, and J.W.C. Vries, "Heat Generation in Multilayer Piezoelectric Actuators," Journal of the American Ceramic Society **79**(12), 3193–3198 (2018).
[11] M.S. Senousy, R.K.N.D. Rajapakse, D. Mumford, and M.S. Gadala, "Self-heat generation in piezoelectric stack actuators used in fuel injectors," Smart Mater Struct **18**(4), 45008 (2009).
[12] S. Trolier-McKinstry, and P. Muralt, "Thin Film Piezoelectrics for MEMS," J Electroceram **12**(1), 7–17 (2004).
[13] A. Dangi, C.Y. Cheng, S. Agrawal, S. Tiwari, G.R. Datta, R.R. Benoit, R. Pratap, S. Trolier-McKinstry, and S.-R. Kothapalli, "A Photoacoustic Imaging Device Using Piezoelectric Micromachined Ultrasound Transducers (PMUTs)," IEEE Trans Ultrason Ferroelectr Freq Control **67**(4), 801–809 (2020).
[14] R.H.T. Wilke, S. Trolier-McKinstry, P.B. Reid, and D.A. Schwartz, in *Proc.SPIE* (2010), p. 78030O.
[15] R.H.T. Wilke, R.L. Johnson-Wilke, V. Cotroneo, W.N. Davis, P.B. Reid, D.A. Schwartz, and S. Trolier-McKinstry, "Sputter deposition of PZT piezoelectric films on thin glass substrates for adjustable x-ray optics," Appl Opt **52**(14), 3412–3419 (2013).
[16] T. Peters, C. Cheng, G.A. Rossetti Jr, and S. Trolier-McKinstry, "Thermal stress accommodation in dip cast lead zirconate-titanate ferroelectric films on flexible substrates," Journal of the American Ceramic Society **105**(6), 4058–4070 (2022).
[17] D. Wang, S. Dursun, L. Gao, C.S. Morandi, C.A. Randall, and S. Trolier-McKinstry, "Fabrication of bimorph lead zirconate titanate thick films on metal substrates via the cold sintering-assisted process," Acta Mater **195**, 482–490 (2020).
[18] K. Gotoh, H. Tamura, H. Takauchi, and A. Yoshida, "Pt/PZT/n-$SrTiO_3$ Ferroelectric Memory Diode," Jpn J Appl Phys **35**(1R), 39 (1996).
[19] N. Bassiri-Gharb, I. Fujii, E. Hong, S. Trolier-McKinstry, D. V Taylor, and D. Damjanovic, "Domain wall contributions to the properties of piezoelectric thin films," J Electroceram **19**(1), 49–67 (2007).
[20] J.S. Lundh, W. Zhu, Y. Song, S.W. Ko, C. Fragkiadakis, P. Mardilovich, S. Trolier-McKinstry, and S. Choi, "Local measurements of domain wall-induced self-heating in released $PbZr_{0.52}Ti_{0.48}O_3$ films," J Appl Phys **128**(21), 214102 (2020).
[21] C. Fragkiadakis, S. Sivaramakrishnan, T. Schmitz-Kempen, P. Mardilovich, and S. Trolier-McKinstry, "Heat generation in PZT MEMS actuator arrays," Appl Phys Lett **121**(16), 162906 (2022).
[22] M. Wallace, "Performance of PZT Based MEMS Devices with Integrated ZnO Electronics," Ph.D. thesis, the Pennsylvania State University, United States, Pennsylvania, (2016), pp. 17–21.
[23] C. Cheng, "Piezoelectric micromachined ultrasound transducers using lead zirconate titanate films," Ph.D. thesis, the Pennsylvania State University, December, (2021), pp. 30–32.
[24] J.S. Lundh, Y. Song, B. Chatterjee, A.G. Baca, R.J. Kaplar, A.M. Armstrong, A.A. Allerman, B.A. Klein, D. Kendig, H. Kim, and S. Choi, "Device-Level Multidimensional Thermal Dynamics with Implications for Current and Future Wide Bandgap Electronics," J Electron Packag **142**(3), (2020).

[25] S. Choi, E.R. Heller, D. Dorsey, R. Vetury, and S. Graham, "Thermometry of AlGaN/GaN HEMTs using multispectral Raman features," IEEE Trans Electron Devices **60**(6), 1898–1904 (2013).
[26] T. Beechem, A. Christensen, S. Graham, and D. Green, "Micro-Raman thermometry in the presence of complex stresses in GaN devices," J Appl Phys **103**(12), 124501 (2008).
[27] J.R. Serrano, L.M. Phinney, and S.P. Kearney, "Micro-Raman thermometry of thermal flexure actuators," Journal of Micromechanics and Microengineering **16**(7), 1128 (2006).
[28] S.K. Oh, J.S. Lundh, S. Shervin, B. Chatterjee, D.K. Lee, S. Choi, J.S. Kwak, and J.-H. Ryou, "Thermal Management and Characterization of High-Power Wide-Bandgap Semiconductor Electronic and Photonic Devices in Automotive Applications," J Electron Packag **141**(2), (2019).
[29] Y. Song, A. Bhattacharyya, A. Karim, D. Shoemaker, H.-L. Huang, S. Roy, C. McGray, J.H. Leach, J. Hwang, S. Krishnamoorthy, and S. Choi, "Ultra-Wide Band Gap Ga2O3-on-SiC MOSFETs," ACS Appl Mater Interfaces **15**(5), 7137–7147 (2023).
[30] J. Dallas, G. Pavlidis, B. Chatterjee, J.S. Lundh, M. Ji, J. Kim, T. Kao, T. Detchprohm, R.D. Dupuis, S. Shen, S. Graham, and S. Choi, "Thermal characterization of gallium nitride p-i-n diodes," Appl Phys Lett **112**(7), 73503 (2018).
[31] J.S. Lundh, "Thermomechanical Analysis of Emerging Microsystems Using Raman Spectroscopy," Ph.D. thesis, the Pennsylvania State University, December, (2021), pp. 19-39.
[32] M. Ozgul, S. Trolier-McKinstry, and C.A. Randall, "Fatigue induced effects on bipolar strain loops in PZN-PT piezoelectric single crystals," J Electroceram **20**(3), 133–138 (2008).